Journal of Power Sources 195 (2010) 3597–3604

Contents lists available at ScienceDirect

Journal of Power Sources

journal homepage: www.elsevier.com/locate/jpowsour

Simultaneous measurement of current and temperature distributions in a proton exchange membrane fuel cell

Guangsheng Zhang[a], Liejin Guo[a], Lizhong Ma[a], Hongtan Liu[a,b,*]

[a] State Key Laboratory of Multiphase Flow in Power Engineering, Xi'an Jiaotong University, Xi'an, Shaanxi 710049, China
[b] Department of Mechanical and Aerospace Engineering, University of Miami, Coral Gables, FL 33124, USA

ARTICLE INFO

Article history:
Received 30 October 2009
Received in revised form 2 December 2009
Accepted 3 December 2009
Available online 29 December 2009

Keywords:
Proton exchange membrane fuel cell (PEMFC)
PEM
Current distribution
Temperature distribution
Simultaneous measurement

ABSTRACT

Using a specially designed current distribution measurement gasket in anode and thin thermocouples between the catalyst layer and gas diffusion layer (GDL) in cathode, in-plane current and temperature distributions in a proton exchange membrane fuel cell (PEMFC) have been simultaneously measured. Such simultaneous measurements are realized in a commercially available experimental PEMFC. Experiments have been conducted under different air flow rates, different hydrogen flow rates and different operating voltages, and measurement results show that there is a very good correlation between local temperature rise and local current density. Such correlations can be explained and agree well with basic thermodynamic analysis. Measurement results also show that significant difference exists between the temperatures at cathode catalyst layer/GDL interface and that in the center of cathode endplate, which is often taken as the cell operating temperature. Compared with separate measurement of local current density or temperature, simultaneous measurements of both can reveal additional information on reaction irreversibility and various transport phenomena in fuel cells.

1. Introduction

It is well known that current density is not uniform in a proton exchange membrane fuel cell (PEMFC), and such non-uniformity has significant negative effects on both its overall performance and durability. Thus, in situ measurements of local parameters are essential for better understanding of this issue and for optimization of PEMFC design and operation. Various in situ local diagnostic techniques have been developed, including measurements of current distribution, temperature distribution, membrane water content distribution, liquid water distribution and species concentration distribution, etc. [1].

Among the various in situ diagnostic techniques, much attention has been paid to local current measurements since local current density is a straightforward indicator of local performance. Other valuable information, such as reactant shortages, membrane dryness and electrode flooding, can also be deducted approximately from the distribution of local current density. Segmentation [2–14] or semi-segmentation [15–17] of current collector/flow field plate and fabrication of subcells electrically isolated from main cell [18–21] are widely used approaches to current distribution measurement in PEMFC. Adoption of embedded resistors [18,22] or Hall sensors [23] were also proved effective. Indirect deduction from current-induced magnetic field measurement [24,25] or from potential distribution measurement [26,27] and separate measurement of current density under the channel and the shoulder with partially catalyzed electrode [28,29] are recently developed methods with special features.

A number of temperature distribution measurement methods have been also developed. Insertion of commercially available or specially fabricated fine temperature sensors into different positions in PEMFC, including thermocouples [30–38], thermistor [39,40], in-fiber Bragg grating sensor [41] and bandgap temperature sensor [42], is a most widely used approach. Infrared thermography is another important technique for temperature distribution measurement [43–46]. Measurement of gas temperature along the flow channel with tunable diode laser absorption spectroscopy was also demonstrated [47].

It is well known that local temperature in PEMFC is intimately related to local performance because temperature has significant effects on electrochemical reaction kinetics while local current density determines the local heat generation rate and thus the local temperature. Furthermore, some critical phenomena in PEMFC, such as water flooding, membrane dehydration, and even cell failure due to overheating, all depend on both local temperature and local current density. Therefore, compared with independent measurement of either local current distribution or local temperature distribution, simultaneous measurement of both can provide addi-

* Corresponding author at: State Key Laboratory of Multiphase Flow in Power Engineering, Xi'an Jiaotong University, Xi'an, Shaanxi 710049, China.
Tel.: +86 2982665591.
E-mail addresses: hongtanliu@mail.xjtu.edu.cn, hliu@miami.edu (H. Liu).

0378-7753/$ – see front matter © 2009 Elsevier B.V. All rights reserved.
doi:10.1016/j.jpowsour.2009.12.016

tional information and lead to better understanding the various phenomena in a fuel cell. Besides, the relationship between local temperature and current density obtained from the simultaneous measurement can reveal more fundamental information about reaction irreversibility and various transport phenomena in a fuel cell.

Although numerous in situ measurements of current distribution and temperature distribution [2–47] have been reported, simultaneous measurements of current and temperature distribution in PEMFC are very limited. Hakenjos et al. [43,44] designed a special PEMFC allowing simultaneous evaluation of current, temperature and water distributions in the fuel cell. Current distribution was measured with segmented anode flow field and temperature was measured with infrared thermography through an optical window in the cathode end plate. Due to the limitation of the technique, it was only possible to measure temperature distribution on the surface of cathode gas diffusion layer (GDL). Maranzana et al. [35] developed a single PEMFC to measure current and temperature distribution along the gas channels. They observed that the temperature field was strongly correlated with the current distribution and both depended strongly on water management. However, the thermocouples were inserted in the ribs of the flow field plates and thus it was not possible to measure the temperature close to the catalyst layer.

A large portion of the heat generated in a PEMFC occurs in the cathode catalyst layer and its local temperature is inherently related to its local current density and overpotential. Thus in order to understand the relationship between local temperature and current density, for simultaneous measurements of temperature and current density the ideal location for thermocouples is the cathode catalyst layer. Therefore, the objectives of this work are (a) to develop a technique to simultaneously measure local current density and the temperature in the cathode catalyst layer and (b) to find the relationship between local temperature and current density.

2. Experimental methodology

2.1. The experimental system

A single PEMFC with an active area of 4 cm × 4 cm was used for all measurements in this work. Fig. 1 shows schematically the PEMFC assembly. MEA in the fuel cell consists of a catalyst coated membrane (CCM, Shanghai Pearl Hydrogen Power Source, China) and two identical carbon paper GDLs with microporous layer (Spectracarb™ 2050-L carbon paper, Spectracorp, USA). Thickness of the membrane is about 50 μm and that of GDL is 200 μm. Catalyst loading of the CCM is 0.3 mg Pt cm^{-2} at the anode and 0.5 mg Pt cm^{-2} at the cathode. Geometric parameters of the MEAs are shown in Table 1.

Table 1
Geometric parameters of the experimental PEMFC.

Channel length (mm)	39
Channel width (mm)	2
Channel depth (mm)	1
Shoulder width (mm)	2
Flow field plate thickness (mm)	13
Current collector thickness (mm)	1.5
Endplate thickness (mm)	19
Number of channels	10
Number of shoulders	9
MEA active area (cm^2)	4 × 4
Membrane thickness (mm)	0.05
CL thickness (mm)	0.01
GDL thickness (mm)	0.20

A pair of graphite flow field plates with serpentine flow field pattern was used in the fuel cell. The flow field at the cathode is identical to that at the anode and parallel flow (co-flow) is used. Channel width, channel depth and shoulder width are 2 mm, 1 mm and 2 mm, respectively. There are 10 channels and 9 shoulders in every flow field plate. Details of the geometric parameters of the flow field plates are shown in Table 1.

A fuel cell test station (FCTS-16, Fuel Cell Technologies, Inc., USA) is used to control operating parameters of the fuel cell, including gas flow rates, gas humidification temperatures, backpressure, cell operating temperature and cell operating voltage. Details about this fuel cell test station are described previously [17].

Hydrogen (purity >99.99%) is supplied as fuel by a hydrogen generator from pure water electrolysis and air is supplied as oxidants by an air pump with filtering and drying system.

2.2. Measurement method

Temperature distributions in the experimental PEMFC are measured by 10 very thin T type thermocouples (RQB-0.08, Captec Enterprise, France) placed between catalyst layer and GDL in cathode side considering that most heat is generated in the cathode catalyst layer which should have the highest temperature in the through-plane direction. Together with Fig. 1, Fig. 2 shows the positions of the 10 thermocouples. It can be seen that there is

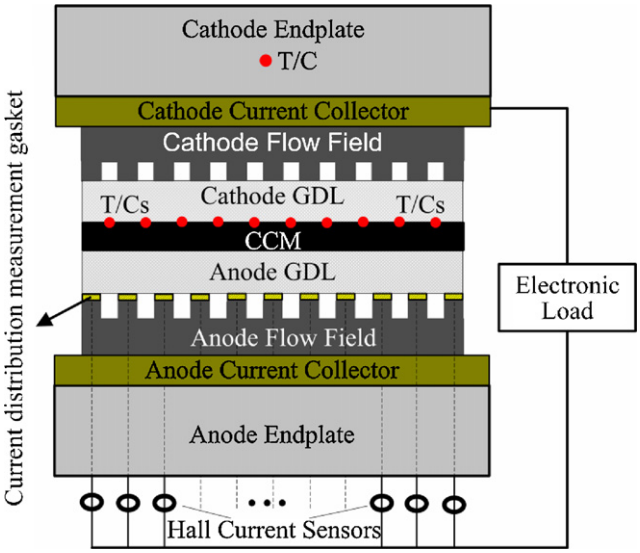

Fig. 1. Schematic diagram of the experimental PEMFC.

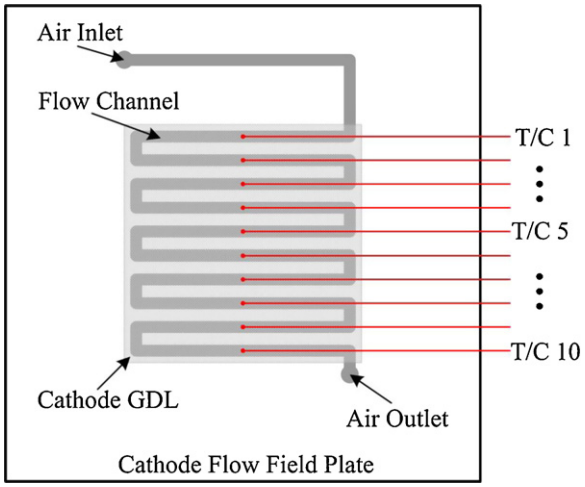

Fig. 2. Schematic positions of thermocouples.

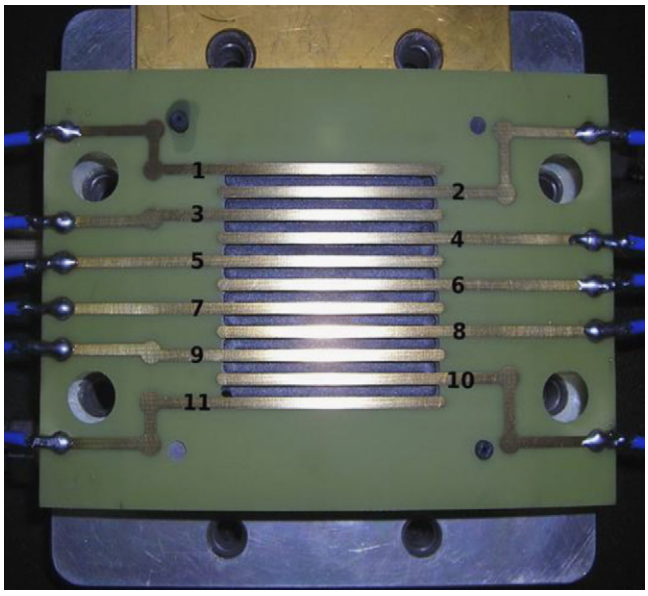

Fig. 3. Photograph of the current distribution measurement gasket placed on the anode flow field plate.

a thermocouple above each channel and the measuring tip is at the center of the channel along flow direction. The thermocouples, insulated with perfluoroalkoxy (PFA), having a cross-dimension of 0.1 mm (thickness) and 0.2 mm (width) including insulation layer, are very thin compared with the channel width of 2 mm. Temperatures measured by the 10 thermocouples are recorded by a 16-bit multi-channel data acquisition device (MX100, Yokogawa Electric Corp., Japan) at a sampling rate of one time per second for each local temperature.

In many studies, the temperature measured by a thermocouple placed in the cathode endplate (CEP), as shown in Fig. 1, is taken as the cell operating temperature. In this study, this temperature is named cathode endplate temperature (T_{CEP}) to differentiate it from the local temperatures measured at the cathode catalyst layer/GDL interface.

To provide specific boundary conditions for the temperature measurement, cathode endplate temperature of the cell is kept stable with a temperature controller (Series 1600, Love Controls Division, Dwyer Instruments, Inc., USA), which controls two heating rods inserted in the endplates for heating and a fan for cooling.

Current distributions in the experimental PEMFC are measured with the current distribution measurement gasket technique, details of which are described in previous publication [17]. Fig. 1 shows briefly how the technique works and Fig. 3 is a photograph of the current distribution measurement gasket placed on the anode flow field plate. As is shown in Figs. 1 and 3, the current distribution measurement gasket fabricated with printed circuit board (PCB) technology is placed between anode GDL and anode flow field plate, with current conducting gold plated copper strips in direct contact with the GDL. The current conducting strips are insulated from each other and from the flow field plate because the gasket substrate is nonconductive. Therefore, instead of passing through flow field plate in a whole, the individual current in the anode passes through each conducting strip separately. Thicknesses of the gasket substrate layer, the copper layer and the gold layer are about 0.2 mm, 0.03 mm and 0.002 mm, respectively.

Different from the experimental system in previous work on current distribution measurement [17,48–50], in which a multi-channel potentiostat was used to control the operating voltages and measure the local currents, in this study the electronic load (N3306A, Agilent, USA) embedded in the fuel cell test station is used to control the operating voltage and Hall sensors (LTSR 6-NP, LEM, Switzerland) are used to measure the local currents in a non-contact way. The range of the Hall sensors is set to be 2 A (lowest available range) for high accuracy. The voltage output of the Hall sensor is proportional to the current passing through it and it is converted to current value by the data acquisition software. Both voltage and converted current values of each Hall sensor are recorded by the same data acquisition device used for temperature recording at a sampling rate of twice per second, thus simultaneous measurements of current density and temperature were ensured.

2.3. Experimental data reduction

As can be seen in Figs. 2 and 3, there are 10 gas channels and 9 shoulders in the flow field. For all experiments in this work, the experimental PEMFC stands vertically with reactant gas inlets on the top and outlets on the bottom of the flow field. As is shown in Fig. 2, the 10 thermocouples are numbered from T/C 1 to T/C 10 along the direction from inlet to outlet, corresponding to the 10 channels. Fig. 3 shows that the 11 current conducting strips in the current distribution measurement gasket are numbered from 1 to 11, with number 2 to number 10 corresponding to the 9 shoulders.

Among the 11 current conducting strips shown in Fig. 3, each of the 9 strips from number 2 to number 10 collects current from one shoulder and two half-channels, which represents an active area of 1.6 cm^2, and the local current density can be calculated from measured local current divided by the area of 1.6 cm^2. For current conducting strips number 1 and number 11, situated on the edges of the MEA, each of them covers a smaller active area than the other 9 strips, collecting less currents, and the exact covering area is hard to calculate because it is difficult to keep the edge of the MEA perfectly match the edge of the flow field. Therefore, local currents number 1 and number 11 will not be used in the following presentation. Even though the currents collected by strips number 1 and number 11 are not used in the final results analysis, these two strips were still connected in the measurement system to minimize extra currents flow through the adjacent strips. In order to minimize edge effect and focus on the trend of the temperature distribution, the temperatures measured by T/C 1 and T/C 10 at both ends will not be used in the result presentation, either.

Considering that this work studies the current and temperature distributions in steady state, average values during a period of 5 min instead of transient values at some specific time will presented in following results for both current distribution and temperature distribution. The 5-min-period starts only when the local currents and temperatures become stable and last for a while.

Note that any modification of PEMFC for current or temperature measurement may have some influences on the overall and local performance of a PEMFC. As indicated in Figs. 1 and 3, insertion of the current distribution measurement gasket will cause an increase in the gas channel depth which will lead some change in gas velocity. Insertion of the thermocouples between catalyst layer and GDL in cathode could also increase mass transfer resistance in the areas directly blocked by the thermocouples, but the thermocouple is so thin, and it is inserted in under the channel, any such effects would be negligible since concentration losses in under channel is usually negligible [29]. Even if the performances of the instrumented cell would be different from those for an un-instrumented cell, the general relationship between local current density and local temperature would not be affected, which is the focus of this study. Moreover, compared with other reported methods, the current distribution measurement method used in this work requires minimum modification of a PEMFC, and placing the measurement gasket at the anode makes its influence on the trend of current distribution in the in-plane direction almost negligible according

to a numerical study on the influence of segmentation of current collector by Natarajan and Van Nguyen [8].

Regarding the influence on the temperature distribution, which is mainly due to the lower thermal conductivity of the PCB-based gasket, it can be negligible, too. Firstly, it is the temperature distribution in the in-plane direction that is studied, with structure and material kept the same for each measurement location. Secondly, it is the steady-state distribution that is measured. Therefore, the influence due to lower thermal conductivity of the gasket in the through-plane direction would be little. In addition, thermocouples are placed between the cathode catalyst layer and the GDL, where they are closest to the electrochemical reaction region generating most heat. At this location, the effects of other material on the measured temperature are further reduced.

3. Results and discussion

With the measurement method described above, current and temperature distributions in the experimental PEMFC under different operating conditions were measured and analyzed. In the base case, the flow rates for hydrogen and air are 200 Nml min^{-1} (equivalent to stoichiometry of 1.8 for average current density at 1000 mA cm^{-2}) and 1200 Nml min^{-1} (equivalent to stoichiometry of 4.5 for average current density at 1000 mA cm^{-2}), respectively, and the anode and cathode humidification temperatures as well as the cathode endplate temperature are all 50 °C. The flowrates chosen in base case are quite large to minimize the effect of insufficient reactant. When the focus is to study the effects of a specific parameter, only this parameter is varied and all the other parameters are kept unchanged. For all measurements, both the anode and cathode vents were directly connected to atmosphere to keep the backpressure at 1 atm.

3.1. Different air flow rates

Current and temperature distributions in the experimental PEMFC at different air flow rates are plotted in Fig. 4. As is shown in Fig. 4(a), when the air flow rate is very low at 60 Nml min^{-1}, equivalent to an average current density of 200 mA cm^{-2}, the local current density decreases gradually along the direction from gas inlet to gas outlet. This is caused by the gradual consumption of oxygen along the flow direction in a serpentine flow field. The local current density becomes almost zero near the outlet, indicating oxygen depletion. Fig. 4(b) shows that temperature distribution presents a similar trend of decreasing gradually along the flow direction for air flow rate of 60 Nml min^{-1}. As the air flow rate increases, all the local current densities increase accordingly due to increased local oxygen concentrations and the current distribution curve becomes more uniform. This trend is consistent with the previous results on current distribution measurement in PEMFC with serpentine flow field [17,49]. It can be seen from Fig. 4(b) that the local temperatures also increase with increasing air flow rate and the temperature distribution becomes more uniform similar to the current distribution.

It is interesting to note that when the air flow rate increases from 900 Nml min^{-1} to 1500 Nml min^{-1}, as is shown in Fig. 4(a), the local current densities increase significantly, whereas the local temperatures hardly change as shown in Fig. 4(b). This phenomenon can be attributed to the convective cooling effect of the air. Even though heat generation rate is higher at higher current density, higher air flow rate also has a higher heat transfer capability. At some point, these two opposite effects on temperature at the measurement location are equal and the temperature does not change significantly.

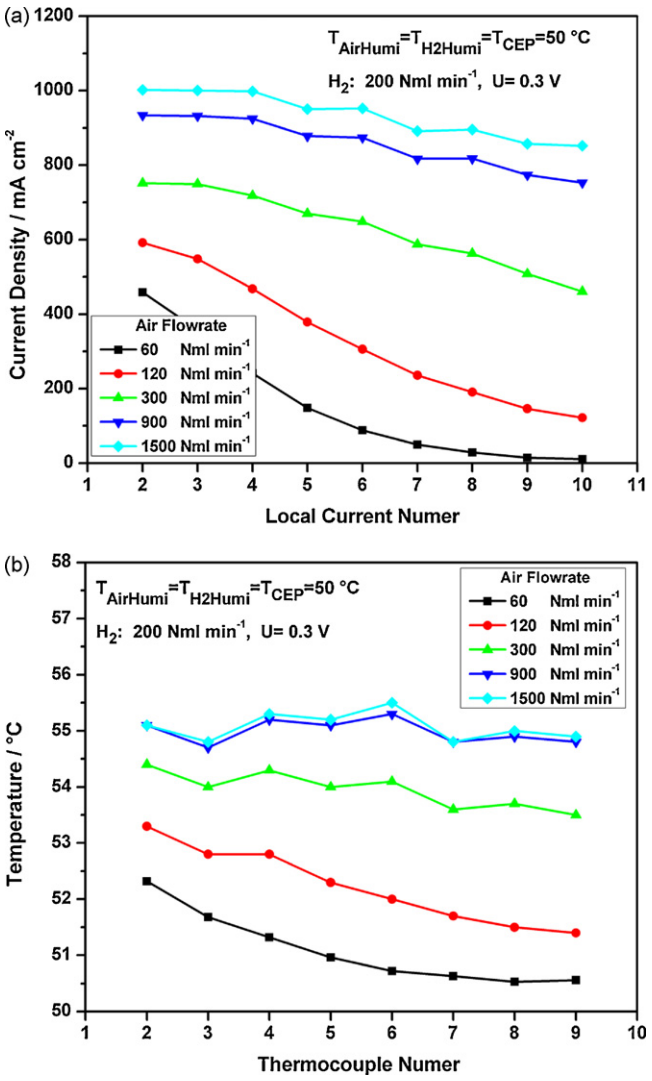

Fig. 4. (a) Current distributions and (b) temperature distributions at different air flow rates.

3.2. Different hydrogen flow rates

Current and temperature distributions at different hydrogen flow rates were also investigated and the results are presented in Fig. 5. At low flow rates (from 30 Nml min^{-1} to 100 Nml min^{-1}), both local current densities and temperatures increase significantly with hydrogen flow rate, while at sufficiently high flow rate from 100 Nml min^{-1} to 200 Nml min^{-1}, both current and temperature change slightly along the flow direction. It is also apparent from Fig. 5 that when hydrogen supply is insufficient, it is consumed quickly in the upstream and the down stream becomes starved of hydrogen. It is very interesting to note when the cell is starved of hydrogen, the local current density decreases more smoothly than the local temperature. This is actually caused by the lateral current conduction due to the very high current density gradient in the transition region. Since the local current is collected after it passes through the GDL and the GDL has very high lateral electrical conductivity, when the current generated under one measurement strip is much lower than its adjacent one, significant lateral electrical conduction exists in the GDL. On the other hand, the local temperature is measured by thermocouples inserted between the catalyst layer and the GDL, the effect of lateral heat conduction is not significant. Therefore, in such situation, the local temperature is

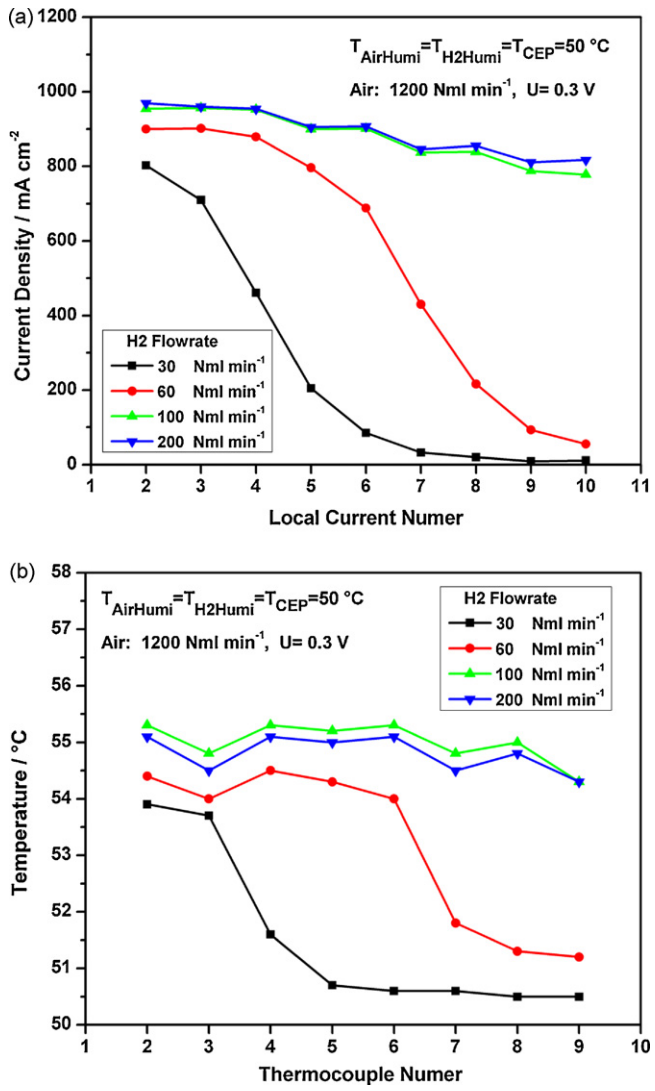

Fig. 5. (a) Current distributions and (b) temperature distributions at different hydrogen flow rates.

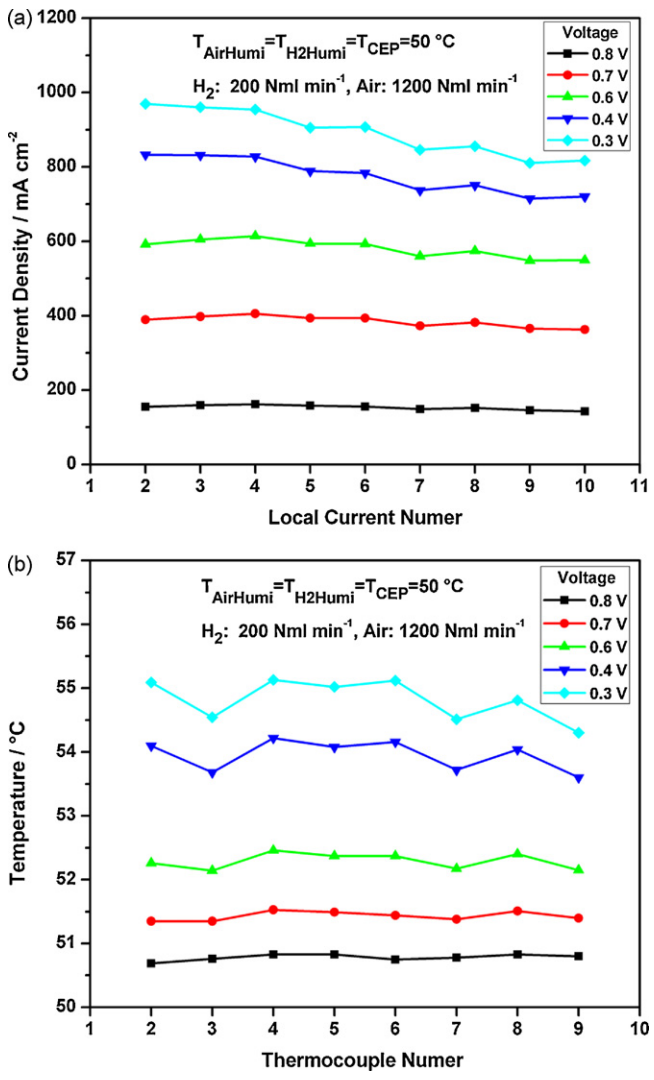

Fig. 6. (a) Current distributions and (b) temperature distributions at different cell operating voltages with sufficient air supply.

actually a better indication of local reaction rate than the measured local current density.

Although there are similarities between the results at different hydrogen flow rates and those at different air flow rates, the differences between them are also apparent. First, when air flow rate is low, the local current density starts rather low (about 460 mA cm^{-2} for air flow rate of 60 Nml min^{-1}, shown in Fig. 4) and gradually decreases along the flow direction. While when the hydrogen flow rate is low at 30 Nml min^{-1}, the local current density starts much higher (about 800 mA cm^{-2}, shown in Fig. 5) and decreases much more abruptly along the flow direction. This difference can be attributed to the much faster hydrogen reduction kinetics and higher hydrogen diffusivity.

Second, the local current densities increase markedly when air flow rate increases from 900 Nml min^{-1} (equivalent to 3100 mA cm^{-2}) to 1500 Nml min^{-1} as is shown in Fig. 4(a), while they increase very little when hydrogen flow rate increases from 100 Nml min^{-1} (equivalent to 900 mA cm^{-2}) to 200 Nml min^{-1} as is shown in Fig. 5. It suggests that hydrogen flow rate of 100 Nml min^{-1} is already sufficient for the experimental PEMFC under such operating conditions due to the faster transfer and reaction of hydrogen than oxygen in the air and further increasing hydrogen flow rate does not improve the cell performance.

Fig. 5(b) shows that the local temperatures with hydrogen flow rate of 200 Nml min^{-1} are lower than those with hydrogen flow rate of 100 Nml min^{-1}. This is similar to the case when air flow rate increases from 900 Nml min^{-1} to 1500 Nml min^{-1} discussed above. In this case, increase in hydrogen flow rate does not leads to a higher current density, but the higher flow rate causes higher convective heat transfer, thus causes lower local temperature.

3.3. *Different cell voltage*

It is well known that operating voltage has significant effects on both overall and local current density of PEMFC. Lower operating voltage means higher overpotential, which results in higher current density and lower efficiency, both causes higher heat generation rate. Therefore, current distribution and temperature distribution in the experimental PEMFC under different operating voltages were investigated. Fig. 6 shows the results with sufficient air supply of 1200 Nml min^{-1} and Fig. 7 the results with insufficient air supply of only 120 Nml min^{-1}.

As is shown in Fig. 6(a), all the local current densities increase significantly as the operating voltage decreases and the local current density decreases noticeably from inlet to outlet at low operating voltages, which agrees well with previous results on current distribution measurement [5,17].

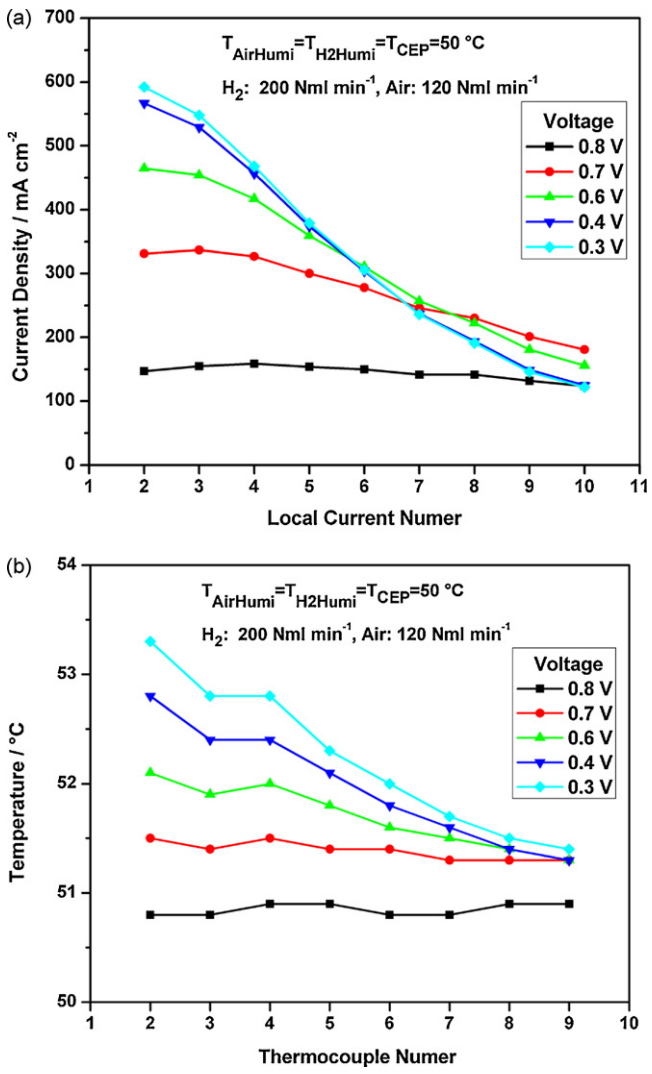

Fig. 7. (a) Current distributions and (b) temperature distributions at different cell operating voltages with insufficient air supply.

Lower operating voltage results in higher local current density and higher local heat flux, and local temperatures should increase accordingly. This trend is verified by the temperature distribution results shown in Fig. 6(b), in which all the local temperatures increase significantly with decreasing operating voltages, similar to the variation of local current densities. Comparison of Fig. 6(a) and (b) shows that the temperature distribution trend generally corresponds to that of current distribution, indicating good correlations between them.

It can be seen from Fig. 7 that the results with insufficient air supply show similar trend to those in Fig. 6: local current densities increase with decreasing operating voltage and variation of local temperature distribution follows that of current distribution very well. The differences between Figs. 7 and 6 are that local current densities and local temperatures in Fig. 7 are lower and they decrease more quickly along the flow direction due to much lower oxygen concentration and lower gas flow velocity.

It can also be seen from Fig. 6 that when the local current densities are about 1000 mA cm^{-2}, the local temperatures measured at the cathode catalyst layer/GDL are about 5 °C higher than the cathode endplate temperature, T_{CEP}, which is often taken as the fuel cell operating temperature in many studies. When oxygen is used as oxidants and PEMFC operates at higher current density, the temperature difference should be even larger. This result indicates that caution must be taken when using the temperature in the end plates, or the collector plate to monitor fuel cell operations, especially in high current density region and/or at high operating temperatures.

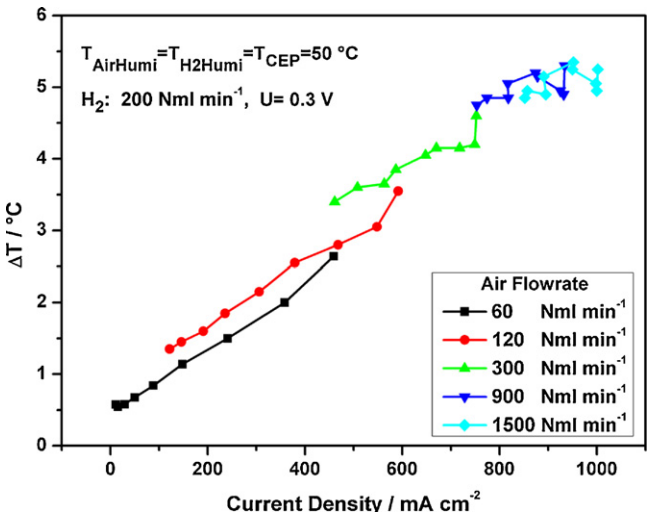

Fig. 8. Correlation between current distribution and temperature distribution at different air flow rates.

3.4. Correlation between local current density and temperature

The results presented in Figs. 4–7 show that the trends of local temperature and current density distributions are very similar. To clearly show the relationship between them, plots showing temperature versus current density are to be produced. However, as shown in Figs. 1–3, local temperatures are measured under the flow channels and local currents are collected above flow field shoulders, i.e. the locations for temperature and current measurements are staggered. In order to plot temperature verses current density, the measured local temperatures were interpolated linearly to the positions of local current densities. Additionally, instead of local temperature, the temperature rise, ΔT, defined as the difference between the measured local temperature and T_{CEP} (50 °C in this work), is used in the presentations.

Figs. 8 and 9 show the relationships between the local temperature rise and local current density at the same cell voltage and at

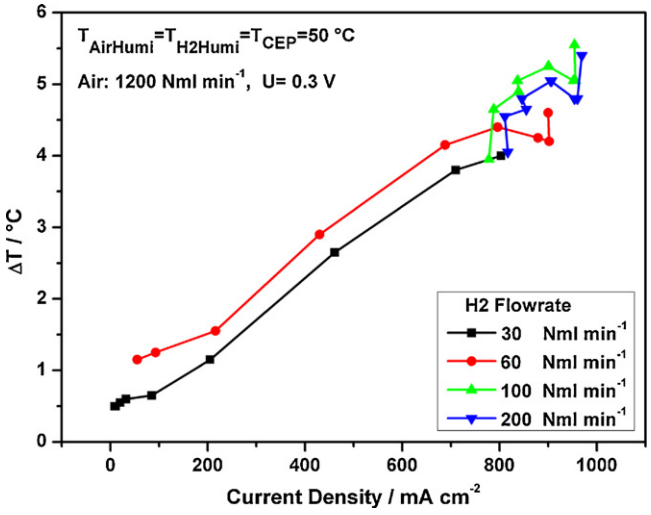

Fig. 9. Correlation between current distribution and temperature distribution at different hydrogen flow rates.

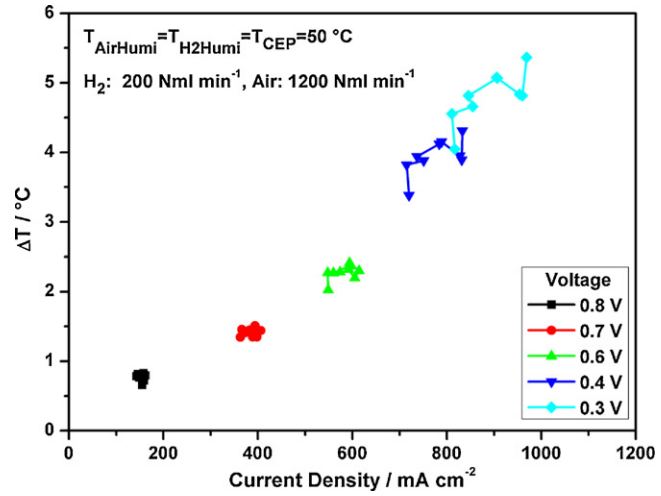

Fig. 10. Correlation between current distribution and temperature distribution at different cell voltages with sufficient air supply.

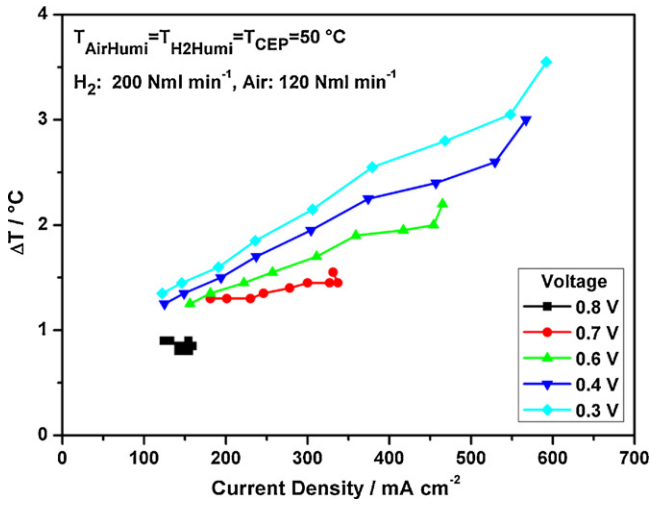

Fig. 11. Correlation between current distribution and temperature distribution at different cell voltages with insufficient air supply.

different air and hydrogen flow rates, respectively. It can be clearly seen that the local temperature rise increases almost linearly with current density for every specific gas flow rate when the cell voltage is kept constant. It can be seen also that the slope of curves at different flow rates are almost the same.

The linear correlation can be explained with basic thermodynamic analysis on heat generation in PEMFC. It is known that local electric energy output (P_{el}) and local heat generation (q) in PEMFC can be simply expressed as

$$P_{el} = jU \tag{1}$$

$$q = j(E_{thermo} - U) \tag{2}$$

where j represents the local current density, U the cell operating voltage, and E_{thermo} the thermo neutral potential, which is about 1.48 V for hydrogen PEMFC at standard temperature and pressure (STP) based on the high heating value of hydrogen.

Eqs. (1) and (2) suggest that if the cell operating voltage is kept constant everywhere, which is true for the case shown in Figs. 8 and 9 with a fixed operating voltage of 0.3 V, the local heat generation is proportional to the local current density. It shows that the correlation results can be explained and agree well with the basic thermodynamic analysis.

It can be noticed by careful observation of Fig. 8 that slopes of the correlation curve decrease as air flow rate increases. It can be attributed to the increased convective cooling effects of higher air flow rate.

Figs. 10 and 11 show the correlation results at different cell operating voltages with sufficient air supply (1200 Nml min^{-1}) and insufficient air supply (120 Nml min^{-1}), respectively. It can be seen that slopes of the correlation curve increases as the operating voltage decreases. The trend is more apparent in Fig. 11 than that in Fig. 10 due to the low air flow rate of 120 Nml min^{-1}, where the convective cooling effects are not as significant. This trend can also be explained by the basic thermodynamic analysis shown in Eq. (2). According to Eq. (2), at the same local current density, the lower the operating voltage is, the higher is the heat generation rate, thus the slope of the temperature versus current density curves increases with decreasing cell voltage.

Such good correlations between local temperature and current density could provide foundations for novel in situ diagnostic techniques in fuel cells since local temperature is usually much easier to measure and it could be used to determine local current density [32].

4. Conclusions

Combined with the current distribution measurement gasket technique and high-precision thin thermocouples placed at the cathode catalyst layer/GDL interface, a technique for simultaneous measurements of local current density and temperature in an PEMFC is developed. With this technique, simultaneous measurements are realized in a commercially available experimental PEMFC. From the results of simultaneous measurements under different operating conditions, the following conclusions can be made:

- There exist good correlations between local temperature and local current density.
- The correlations between local temperature and local current density agree very well with basic thermodynamic analysis.
- The slope of the curves for local temperature rise versus local current density increases with decreasing cell operating voltage.
- The effect of convective cooling on local temperature in PEMFC is significant at high reactant flow rates.
- Significant temperature difference exists between cathode catalyst layer and the endplate plate.
- Simultaneous measurement of current and temperature distributions can provide more detailed information than separate measurements.

Acknowledgements

Financial supports from the Chang Jiang Scholars Program of the Ministry of Education of China and the NSFC Fund for Creative Research Groups (Grant No. 50821064) are gratefully acknowledged. The authors thank Mr. Shuanglin Shen for his assistance in conducting some of the experiments.

References

[1] J. Wu, X.Z. Yuan, H. Wang, M. Blanco, J.J. Martin, J. Zhang, Int. J. Hydrogen Energy 33 (2008) 1747–1757.
[2] S.J.C. Cleghorn, C.R. Derouin, M.S. Wilson, S. Gottesfeld, J. Appl. Electrochem. 28 (1998) 663–672.
[3] D.J.L. Brett, S. Atkins, N.P. Brandon, V. Vesovic, N. Vasileiadis, A.R. Kucernak, Electrochem. Commun. 3 (2001) 628–632.
[4] M. Noponen, T. Mennola, M. Mikkola, T. Hottinen, P. Lund, J. Power Sources 106 (2002) 304–312.
[5] M.M. Mench, C.Y. Wang, M. Ishikawa, J. Electrochem. Soc. 150 (2003) A1052–A1059.
[6] Y.G. Yoon, W.Y. Lee, T.H. Yang, G.G. Park, C.S. Kim, J. Power Sources 118 (2003) 193–199.

[7] A. Hakenjos, K. Tuber, J.O. Schumacher, C. Hebling, Fuel Cells 4 (2004) 185–189.
[8] D. Natarajan, T. Van Nguyen, J. Power Sources 135 (2004) 95–109.
[9] A.B. Geiger, R. Eckl, A. Wokaun, G.G. Scherera, J. Electrochem. Soc. 151 (2004) A394–A398.
[10] T. Araki, H. Koori, T. Taniuchi, K. Onda, J. Power Sources 152 (2005) 60–66.
[11] Z. Siroma, N. Fujiwara, T. Loroi, S. Yamazaki, H. Senoh, K. Yasuda, K. Tanimoto, J. Power Sources 172 (2007) 155–162.
[12] M. Schulze, E. Gulzow, S. Schonbauer, T. Knori, R. Reissner, J. Power Sources 173 (2007) 19–27.
[13] D.G. Strickland, S. Litster, J.G. Santiago, J. Power Sources 174 (2007) 272–281.
[14] T. Knori, M. Schulze, J. Power Sources 193 (2009) 308–314.
[15] F.N. Buchi, A.B. Geiger, R.P. Neto, J. Power Sources 145 (2005) 62–67.
[16] R. Eckl, R. Grinzinger, W. Lehnert, J. Power Sources 154 (2006) 171–179.
[17] H. Sun, G. Zhang, L. Guo, H. Liu, J. Power Sources 158 (2006) 326–332.
[18] J. Stumper, S.A. Campbell, D.P. Wilkinson, M.C. Johnson, M. Davis, Electrochim. Acta 43 (1998) 3773–3783.
[19] N. Rajalakshmi, M. Raja, K.S. Dhathathreyan, J. Power Sources 112 (2002) 331–336.
[20] J.F. Wu, B.L. Yi, M. Hou, Z.J. Hou, H.M. Zhang, Electrochem. Solid-State Lett. 7 (2004) A151–A154.
[21] Z.X. Liu, Z.Q. Mao, B. Wu, L.S. Wang, V.M. Schmidt, J. Power Sources 141 (2005) 205–210.
[22] P.C. Ghosh, T. Wuster, H. Dohle, N. Kimiaie, J. Mergel, D. Stolten, J. Power Sources 154 (2006) 184–191.
[23] C. Wieser, A. Helmbold, E. Gulzow, J. Appl. Electrochem. 30 (2000) 803–807.
[24] K.-H. Hauer, R. Potthast, T. Wuster, D. Stolten, J. Power Sources 143 (2005) 67–74.
[25] M. Izumi, Y. Gotoh, T. Yamanaka, ECS Trans. 17 (2009) 401–409.
[26] S.A. Freunberger, M. Reum, J. Evertz, A. Wokaun, F.N. Buchi, J. Electrochem. Soc. 153 (2006) A2158–A2165.
[27] M. Reum, S.A. Freunberger, A. Wokaun, F.N. Buchi, J. Electrochem. Soc. 156 (2009) B301–B310.
[28] L. Wang, H.T. Liu, J. Power Sources 180 (2008) 365–372.
[29] A. Higier, H. Liu, J. Power Sources 193 (2009) 639–648.
[30] M.M. Mench, D.J. Burford, T.W. Davis, Proceedings of the 2003 ASME International Mechanical Engineering Congress & Exposition, vol. 374, 2003.
[31] T. Fabian, J.D. Posner, R. O'Hayre, S.-W. Cha, J.K. Eaton, F.B. Prinz, J.G. Santiago, J. Power Sources 161 (2006) 168–182.
[32] M. Wilkinson, M. Blanco, E. Gu, J.J. Martin, D.P. Wilkinson, J.J. Zhang, H. Wang, Electrochem. Solid-State Lett. 9 (2006) A507–A511.
[33] A.M. Abdullah, T. Okajima, A.M. Mohammad, F. Kitamura, T. Ohsaka, J. Power Sources 172 (2007) 209–214.
[34] T. Fabian, R. O'Hayre, F.B. Prinz, J.G. Santiago, J. Electrochem. Soc. 154 (2007) 910–918.
[35] G. Maranzana, O. Lottin, T. Colinart, S. Chupin, S. Didierjean, J. Power Sources 180 (2008) 748–754.
[36] C.-Y. Wen, G.-W. Huang, J. Power Sources 178 (2008) 132–140.
[37] P.J.S. Vie, S. Kjelstrup, Electrochim. Acta 49 (2004) 1069–1077.
[38] S.-K. Lee, K. Ito, T. Ohshima, S. Noda, K. Sasaki, Electrochem. Solid-State Lett. 12 (2009) B126–B130.
[39] S.H. He, M.M. Mench, S. Tadigadapa, Sens. Actuator A: Phys. 125 (2006) 170–177.
[40] C.Y. Lee, W.J. Hsieh, G.W. Wu, J. Power Sources 181 (2008) 237–243.
[41] N.A. David, P.M. Wild, J. Hu, N. Djilali, J. Power Sources 192 (2009) 376–380.
[42] G. Hinds, M. Stevens, J. Wilkinson, M. de Podesta, S. Bell, J. Power Sources 186 (2009) 52–57.
[43] A. Hakenjos, H. Muenter, U. Wittstadt, C. Hebling, J. Power Sources 131 (2004) 213–216.
[44] A. Hakenjos, C. Hebling, J. Power Sources 145 (2005) 307–311.
[45] R. Shimoi, M. Masuda, K. Fushinobu, Y. Kozawa, K. Okazaki, J. Energy Resour. Technol. 126 (2004) 258–261.
[46] M.H. Wang, H. Guo, C.F. Ma, J. Power Sources 157 (2006) 181–187.
[47] S. Basu, M.W. Renfro, B.M. Cetegen, J. Power Sources 162 (2006) 286–293.
[48] H. Sun, G. Zhang, L. Guo, D. Shang, H. Liu, J. Power Sources 168 (2007) 400–407.
[49] G. Zhang, L. Guo, B. Ma, H. Liu, J. Power Sources 188 (2009) 213–219.
[50] H. Sun, G. Zhang, L. Guo, H. Liu, Int. J. Hydrogen Energy 34 (2009) 5529–5536.